Hyperactive HRAS dysregulates energetic metabolism in fibroblasts from patients with Costello syndrome *via* enhanced production of reactive oxidizing species

Giovanna Carpentieri[1,2], Chiara Leoni[3], Donatella Pietraforte[4], Serena Cecchetti[4], Egidio Iorio[4], Antonio Belardo[5], Daniele Pietrucci[6], Michela Di Nottia[1], Deborah Pajalunga[2], Francesca Megiorni[7], Laura Mercurio[8], Massimo Tatti[2], Simona Camero[9], Cinzia Marchese[7], Teresa Rizza[1], Valentina Tirelli[4], Roberta Onesimo[3], Rosalba Carrozzo[1], Sara Rinalducci[5], Giovanni Chillemi[6], Giuseppe Zampino[3], Marco Tartaglia[1,10,11,*], Elisabetta Flex[2,10,*]

[1]Genetics and Rare Diseases Research Division, Ospedale Pediatrico Bambino Gesù, IRCCS, 00146 Rome, Italy.

[2]Department of Oncology and Molecular Medicine, Istituto Superiore di Sanità, 00161 Rome, Italy.

[3]Center for Rare Diseases and Birth Defects, Department of Woman and Child Health and Public Health, Fondazione Policlinico Universitario A. Gemelli, IRCCS, 00168 Rome, Italy.

[4]Core Facilities, Istituto Superiore di Sanità, 00161 Rome, Italy.

[5]Department of Ecological and Biological Sciences, Università della Tuscia, 01100 Viterbo, Italy.

[6] Department for Innovation in Biological, Agro-food and Forest systems, Università della Tuscia, 01100 Viterbo, Italy.

[7]Department of Experimental Medicine, Sapienza University, 00161 Rome, Italy.

[8]Laboratory of Experimental Immunology, Istituto Dermopatico dell'Immacolata, IRCCS, 00167 Rome, Italy.

[9]Department Maternal Infantile and Urological Sciences, SAPIENZA University, 00161 Rome, Italy.

[10]These authors contributed equally.

[11]Lead contact

*Corrispondence: marco.tartaglia@opbg.net (M.T.), elisabetta.flex@iss.it (E.F.)

Abstract

Germline activating mutations in *HRAS* cause Costello Syndrome (CS), a cancer prone multisystem disorder characterized by reduced postnatal growth. In CS, poor weight gain and growth are not caused by low caloric intake. Here we show that constitutive plasma membrane translocation and activation of the GLUT4 glucose transporter, via ROS-dependent AMPKα and p38 hyperactivation, occurs in CS, resulting in accelerated glycolysis, and increased fatty acid synthesis and storage as lipid droplets in primary fibroblasts. An accelerated autophagic flux was also identified as contributing to the increased energetic expenditure in CS. Concomitant inhibition of p38 and PI3K signaling by wortmannin was able to rescue both the dysregulated glucose intake and accelerated autophagic flux. Our findings provide a mechanistic link between upregulated HRAS function, defective growth and increased resting energetic expenditure in CS, and document that targeting p38 and PI3K signaling is able to revert this metabolic dysfunction.

Introduction

HRAS is a small monomeric GTPase functioning as an intracellular signaling node by activating multiple pathways in response to a wide array of extracellular signals (1). Similarly, to the other members of the RAS subfamily, the protein cycles between active (GTP-bound) and inactive (GDP-bound) states that are finely controlled by GTPase activating proteins (GAPs) and guanine nucleotide exchange factors (GEFs), which stimulate the intrinsic low catalytic activity of the GTPase and GDP dissociation, respectively (2). A narrow spectrum of somatic gain-of-function (GoF) missense mutations affecting codons 12, 13 and 61 are well-known to contribute to

oncogenesis by impairing the GTPase activity of HRAS or its response to GAPs (3). More recently, activating missense mutations in the same gene, either affecting the catalytic activity of the protein or promoting GEF-independent release of GDP, have been identified as the molecular cause of Costello syndrome (CS, OMIM #218040) (4), a rare developmental disorder characterized by intellectual disability, cardiac defects, a distinctive facial gestalt and aged appearance, muscle-skeletal and skin anomalies, poor postnatal growth, and predisposition to certain malignancies (5,6).

Failure to thrive is a major clinical complication of CS, which invariably occurs soon after birth. Commonly, fetal macrosomy is followed by progressive weight loss associated with oro-motor incoordination, which may require enteral nutrition support *via* naso-gastric or gastric tube. While poor swallowing and suckle reflex are considered key events leading to low caloric intake and failure to thrive, poor growth parameters persist along patients' life notwithstanding the improvement of oro-motor skills attained during early childhood. Poor gain weight is often associated with hypoglycemia and hypothalamic/pituitary axis anomalies, with the former supposed to result from growth hormone (GH) and/or cortisol deficiency (7-9). Fasting state hypoglycemia has been documented in CS with or without GH deficiency, in combination with high cholesterol level (10). Of note, recent studies provided evidence of a more complex scenario, in which multiple events are likely to contribute to the growth failure in this disorder, including increased resting energy expenditure and gastro-intestinal problems (10,11). The occurrence of an increased resting basal metabolism in these subjects and low glucose and high cholesterol blood levels suggest the involvement of a still uncharacterized metabolic dysfunction as a driver event contributing to the disorder.

We here show that primary fibroblasts from subjects with CS have accelerated glycolysis and enhanced glucose uptake associated with constitutive plasma membrane translocation and activation of the GLUT4 glucose transporter. These cells show enhanced AMPKα and p38 activation, which results from increased levels of reactive oxidizing species. This oxidative stress is also responsible

for establishing an accelerated autophagic flux in a steady state condition. Finally, we show that the observed metabolic dysfunction in cells can be reverted, at least in part, by treatment with wortmannin.

Results

Fibroblasts of CS patients show an accelerated glycolytic flux not associated with altered mitochondrial function

To explore the underlying mechanisms for metabolic alterations in CS, mass spectrometry-based analysis (12) was performed using primary fibroblast lines obtained from CS patients (n=6) and age-matched healthy donors (n=4). A statistically significant drop of glucose and increased level of glycolytic end-products (*i.e.*, phosphoenolpyruvate, pyruvate and lactate) in patients' fibroblasts compared to control cells were observed (Fig. 1A). This finding, which was indicative of an increased glycolytic activity in the former, was also supported by quantitative ^{1}H-NMR spectroscopy (13-14), which revealed a 2.5-fold increase of intracellular levels of metabolites linked to pyruvate metabolism (*i.e.*, lactate and glycine) in patients' cells (n=5) compared to control cells (n=5) (Fig. S1). A metabolic shift towards the glycolytic pathway may represent a physiologic strategy used by cells to produce energy in response to mitochondrial dysfunction (15). On the other hand, an increased glycolytic flux physiologically occurs in proliferating cells (*e.g.*, cancer cells) even in the presence of oxygen and fully functioning mitochondria (the so-called Warburg effect) (16-19). Based on these considerations, we assayed the mitochondrial activity measuring total content of cellular ATP both in regular and restrictive GAL medium conditions, which did not highlight significant differences in total ATP content in patients' fibroblasts compared to controls cells, ruling out defective ATP production by mitochondrial oxidative phosphorylation (Fig. 1B). Consistent with this finding, indirect evaluation of the OXPHOS status assessed in mitochondria of

three patients by measuring the complex V activity using succinate or malate as substrate showed normal ATP synthesis (Fig. 1C). Overall, these data indicated that the high rates of aerobic glycolysis in CS cells are uncoupled to mitochondrial dysfunction.

A variably enhanced glucose uptake in CS fibroblasts is associated with constitutive activation and plasma membrane translocation of GLUT4

Dependency on glycolysis generally promotes aberrant expression and activation of proteins (*e.g.*, glucose transporters and the serine/threonine protein kinase AKT) positively controlling glucose uptake and metabolism (20). In particular, PI3K/AKT signaling activation following insulin stimulation is known to promote increased GLUT1 levels, which is constitutively targeted to the plasma membrane (PM), and GLUT4 translocation to the PM from the trans-Golgi network, where they favor glucose intake (21,22). Of note, it has been suggested that oncogenic *HRAS* mutations promote prolonged PI3K/AKT signaling after stimulation with EGF in fibroblasts of patients with CS (23). The levels of AKT activation, measured as levels of phosphorylation, were assessed by western Blot (WB) analysis but did not significantly differ with those of control cells, both basally and following EGF or insulin stimulation (Fig. 2A). Since GLUT1 is the major glucose transporter in tissues, and its expression is commonly increased in cancer cells with oncogenic *RAS* gene mutations (24), we evaluated its expression levels by RT-PCR and WB, which were comparable with those observed in control cells (Fig. S2). We therefore analyzed by WB and immunofluorescence (IF) assays the GLUT4 functional status in CS cells, in terms of expression levels, translocation to the plasma membrane and activation. While GLUT4 is mainly expressed in heart, muscle and adipocytes, its expression is observed also in all insulin-responsive tissues, including fibroblasts (25). As assessed by WB and immunofluorescence analyses, we observed an increased level of GLUT4 and its enhanced constitutive translocation to the PM in patients' fibroblasts compared to control cells (Fig. 2B; Fig. S3), which was associated with a variably increased 2DG-glucose uptake (Fig. 2C).

These findings indicated that the accelerated glycolysis characterizing fibroblasts from CS patients in steady state conditions is associated with an enhanced glucose uptake and constitutive PI3K/AKT-independent translocation of GLUT4 to the PM.

CS fibroblasts show ROS-dependent AMPK and p38 activation

A distinct insulin-independent pathway promoting GLUT4 translocation to the cell surface is mediated by AMP-activated protein kinase (AMPK), a metabolic sensor of mammalian cells whose activation is generally triggered by an increased AMP/ATP intracellular ratio; however, GLUT4 translocation to the PM is not sufficient *per se* for glucose intake, which also requires the activation of the glucose transporter through a p38 MAPK-dependent mechanism (26-28). To evaluate this alternative pathway, we carried out WB analyses to assay the activation status of the AMPKα and p38 proteins. A constitutive and significantly increased level of both phospho-AMPKα and phospho-p38 in patients' fibroblasts compared to control cells was observed, pointing to these molecules as the putative proteins mediating the observed enhanced glucose uptake in CS cells (Fig. 3A).

We then explored the mechanism(s) by which the activating germline *HRAS* mutations promote AMPK and p38 activation. It is well established that enhanced RAS signaling is able to induce reactive oxygen species (ROS) production through robust activation of NADPH oxidases (*e.g.*, NOX1 and NOX4) (29-32). Besides the faceted impact of ROS accumulation on multiple cellular processes, increased intracellular ROS levels are known to promote AMPK activity through oxidative modification of the AMPKα subunit (33-35). Similarly, ROS function as second messengers to activate multiple redox-sensitive signaling transduction cascades, including the p38 kinase (36-38). Based on these considerations, ROS levels were assayed in primary fibroblasts from CS patients. ROS and reactive nitrogen species (RNS) content in fibroblast suspensions were measured by EPR spectroscopy, using cyclic hydroxylamine CPH as a partially cell-permeable spin probe oxidized to carboxyproxyl radical ($CP^{\bullet}$) by endogenous oxidants, providing both

extracellular and intracellular free-radical detection (39). A variably higher CP$^{\bullet}$ signal was observed in primary fibroblasts from CS patients compared to age-matched controls (Fig. 3B). Competition assays were performed to characterize the major contributing ROS and RNS species using the three patients' fibroblast lines showing the higher CP$^{\bullet}$ intensity. In these experiments, PEG-Sod and Cat were used as scavengers for superoxide anion ($O_2^{\bullet-}$) and hydrogen peroxide (H_2O_2), respectively, NMA as an inhibitor of $^{\bullet}$NO synthase, and DTPA as a metal chelating agent. CP$^{\bullet}$ intensity in control fibroblasts was significantly decreased by PEG-Sod but unaffected by DTPA, Cat and NMA (Fig. 3C). Similarly, CP$^{\bullet}$ intensity was significantly decreased by PEG-Sod and DTPA, and was unaffected by Cat in fibroblasts from CS patients (Fig. 3C). However, contrarily to controls, pre-incubation with NMA significantly increased CP$^{\bullet}$ formation in all samples from CS fibroblasts (Fig. 3C), indicating that the strong oxidant peroxynitrite ($ONOO^-$), which is formed by $O_2^{\bullet-}$ reacting with $^{\bullet}$NO, was generated in these samples, and that the NMA-mediated decrease of $^{\bullet}$NO concentration favored the reaction of $O_2^{\bullet-}$ or its derived oxidants with the spin probe (Fig. 3C). This finding was validated by monitoring CP$^{\bullet}$ formation in presence of PEG-Sod in cells that had been pre-incubated with NMA, which showed that PEG-Sod did not affect CP$^{\bullet}$ intensity in samples form healthy donors, while significantly decreased radical signal intensity in fibroblasts form CS patients (Fig. 3C). The pro-oxidant status in CS fibroblasts shown by EPR spectroscopy was also supported by mass spectrometry analysis, which documented an increased amount of metabolites associated to the activity of both O2$^{\bullet}$/$^{\bullet}$NO-generating enzyme NOS (*i.e.*, L-arginine and asymmetric dimethylarginine [ADMA]) and O2$^{\bullet}$-generating enzyme xanthine oxidase (hypoxanthine), but also an overproduction of allantoin, a non-enzymatic ROS/RNS-mediated oxidative product of uric acid (Fig. S4), thus sustaining the formation of reactive oxidizing species also by these pathways (40-43). These findings indicate that the increased amounts of ROS and RNS observed in fibroblasts from CS patients include $O_2^{\bullet-}$, $^{\bullet}$NO and likely $ONOO^-$. The antioxidant response of fibroblasts from CS patients to the increased reactive oxidant species was then assayed by mass spectrometry analysis directed to assess the level of glutathione, which is the most

abundant low molecular weight thiol-containing compound within cells. Compared to control cells, fibroblasts from CS patients showed a significantly decreased concentration of reduced glutathione (GSH) (Fig. S5), consistent with an oxidant-dependent increased oxidation of the thiol. Of note, the concentration of the oxidized glutathione (GSSG), which was expected to have higher levels in CS cells as a direct consequence of GSH oxidation, did not differ compared with control cells (Fig. S5). A possible explanation of this finding is linked to the occurrence of reactive oxidizing species-mediated glutathionylation reactions (*i.e.*, formation of reversible mixed disulphides with protein cysteine residues) (44) in CS fibroblasts, which is in line with the observed ROS-mediated activation of AMPK. Overall, these data suggest that an altered redox balance due to increased intracellular ROS and RNS levels promotes the activation of AMPKα and p38 proteins, which in turn drive constitutive plasma membrane translocation and activation of the GLUT4 glucose transporter, resulting in an increased glucose uptake into cells. These findings point to the dysregulated glucose uptake in cells as a major contributing event of the hypoglycemic status in CS patients.

In CS fibroblasts increased glucose uptake promotes fatty acid synthesis and intracellular storage as lipid droplets

Besides the enhanced glucose uptake and accelerated glycolysis, patients' fibroblasts were characterized by a large amount of lipid droplets compared to control cells, visualized by confocal microscopy analysis (Fig. 4A). Moreover, high-performance thin-layer chromatography, which was used to separate neutral lipids from cell extracts, identified higher levels of cholesterol esters (CE) (and triglycerides, with a lesser extent) in cells from CS patients respect to control cells, which represent a major constituting species of lipid droplets (Fig. 4B). As an increased glycolytic flux ensures high levels of acetyl-CoA for fatty acid (FA) synthesis (18,45,46), the increased FA synthesis and their augmented storage as lipid droplets was expected to be related to the increased glucose uptake and accelerated glycolysis observed in patients' cells. To demonstrate a direct link

between augmented glucose intake/metabolism and enhanced lipid droplets formation, patients' and control fibroblasts were starved (18 hours) using medium without glucose and serum. IF analyses and TLC assay documented lipid droplets consumption following starvation in patients' cells, and their prompt regeneration after treatment with medium containing glucose, but not with medium containing serum (Fig. 4C; Fig. S6), confirming a direct link between the levels of glucose uptake and increased lipid droplets accumulation.

CS fibroblasts show enhanced autophagic flux

AMPK is a metabolic sensor of mammalian cells, and it is composed by a catalytic subunit (α) and two regulatory subunits (β and γ). The enzyme, which is activated in response to ATP depletion following glucose deprivation, besides promoting glucose uptake, has a key role in restoring proper energy balance by promoting catabolism *via* autophagy induction (47-49). This catabolic process is triggered by AMPK also following ROS-mediated activation of the enzyme through S-glutationylation of the AMPKα and β subunits (50). Since the higher levels of AMPKα protein activation (51,52), we hypothesized a possible perturbation of the autophagic flux in CS. To test this hypothesis, autophagy was investigated by IF and WB analyses in patients' fibroblasts, using LC3I/II as autophagosomal marker. As shown, we observed a higher level of this marker in patients' cells compared to controls in steady state culture conditions (Fig. 5A). Notably, patients' cells maintained higher levels of LC3 expression/activation also after induction with EBSS for 2, 4 and 8 hours (Fig. 5B). A further increase of LC3 level was observed following treatment with bafilomycin A1, an inhibitor of autophagic vacuoles maturation by impeding fusion between autophagosomes and lysosomes, for 4 hours (Fig. 5B and C), indicating that CS cells are characterized by an accelerated autophagic flux. These data suggest that the increased basal catabolism could contribute to the increased resting energy expenditure observed in patients with CS.

Wortmannin treatment rescues the enhanced glucose uptake and accelerated autophagy in CS fibroblasts

Wortmannin is a fungal metabolite functioning as a potent inhibitor of PI3K complexes but also reported to inhibit p38 MAPK activity (26,53). Since the role of p38 and AMPK-PI3K class III in promoting glucose uptake and autophagic flux in cells, which were both altered in CS fibroblasts, we hypothesized the use of wortmannin to inhibit both processes simultaneously. Treatment with wortmannin was performed to analyze glucose intake, autophagic flux and lipid droplets content in CS fibroblasts maintained in steady state conditions. After 2 hours of treatment (500 nM), a significant decrease of the basal 2-DG glucose uptake in patient's cells was observed, reaching the basal levels observed in control cells (Fig. 6A). Similarly, an inhibitory effect of the treatment (200 nM, 2 hours) was observed on the autophagic flux, as shown by the substantially decrease of LC3II levels in cells cultured with or without EBSS (Fig. 6B). Consistent with the reduced glucose intake, a significant reduction of lipid droplets content in patients' fibroblasts was observed following wortmannin treatment, further supporting the direct association of their production with the increased glucose intake in cells (Fig. 6C). Treatment with wortmannin 200 or 500 nM for two hours did not have effects on cell viability (data not shown).

Discussion

CS is a RASopathy specifically associated with a narrow spectrum of germline missense mutations in *HRAS* (p.Gly12Ser, most commonly) that are rarely observed as somatic events contributing to cancer. These germline mutations are less activating compared to the oncogenic ones, which avoids reaching a lethal signaling threshold during development, but predisposes affected individuals to develop neoplasia during childhood. While major features of CS include distinctive facies, failure to thrive and postnatal reduced growth, cognitive deficits, cardiac and musculoskeletal anomalies, recent clinical observations have provided evidence of an increased resting energy expenditure

associated to low blood glucose and high cholesterol levels as common findings, suggesting the occurrence of a still uncharacterized metabolic dysfunction. Here, we provided evidence that constitutional enhanced HRAS signaling in CS causes a profound metabolic rearrangement *via* enhanced production of ROS that, in turn, promotes increased glucose uptake, accelerated glycolysis, augmented fatty acid synthesis and storage as lipid droplets, and enhanced autophagic flux through ROS-dependent AMPK and p38 activation (Figure 7).

By MS- and NMR-based metabolic fingerprinting and assessment of mitochondrial function, we demonstrated an increased rate of glycolysis in patients' fibroblasts in absence of any evident oxidative phosphorylation defect. Accelerated glycolysis was not dependent on an increased expression of GLUT1, a major glucose transporter in mammalian cells, but was found to be associated with an enhanced expression and constitutive PM translocation of GLUT4 in patients' cells. Consistent with our findings, upregulated RAS signaling has been shown to substantially rewrite energetic metabolism in cells by enhancing both glucose uptake and glycolysis (54-57). Such upregulation of the glycolytic flux is attained by a variegated transcriptional reprogramming of genes encoding key glycolytic proteins and glucose transporters, which is also dependent on the dynamics of RAS functional upregulation (55,57,58). More recently, direct regulation of metabolic enzymes by activated RAS has also been reported (59). While we cannot exclude a contribution of RAS signaling upregulation on glucose uptake and glycolysis exerted at the level of gene expression, our data indicate that chronic upregulation of HRAS signaling indirectly impacts on glucose metabolism by a complex dysregulation of multiple pathways as a result of increased reactive oxidizing species production (60,61).

We observed that the increased glucose uptake in CS cells was associated with an augmented FA synthesis and storage as lipid droplets. In cancer cells, glucose represents a key carbon source for FA synthesis (18,46). During this process, when glucose through glycolysis exceeds bioenergetics need, pyruvate obtained from its final step is first converted to acetyl-CoA in the mitochondrial

matrix where, condensing with oxaloacetate, is used to produce citrate in the TCA cycle (62). When present at high concentrations (as detected by MS in CS cells; Fig. S7), citrate is relocated back into the cytosol to fuel fatty acid and lipid anabolic pathways (63). Consistently, our analyses documented a tight link between increased glucose intake, fatty acid synthesis and their intracellular storage as lipid droplets. We hypothesize that the observed metabolic rearrangements could represent a major contributing factor of the lowering of blood glucose level and increased stored fats observed in patients with CS (10) (Leoni et al., submitted). Of note, a hypoglycemic status was recently reported in a CS knock-in mouse model (*Hras*$^{G12S/+}$) (64). In mice, upregulated Hras function results in an altered metabolic profile with microvesicular hepatic steatosis and growth impairment (lean phenotype) in presence of a high fat diet, while it is associated with early hypoglycemia, low serum levels of β-amino butyric acid and hypoketosis under starvation. Differently from what is observed in mice, however, hepatic steatosis does not occur in CS, and normal concentration of serum β-amino butyric acid after 8 hour-starvation, absence keton bodies in urine and occurrence of normal/low insulin exclude both hypoketotic hypoglycemia and impaired fatty acid oxidation as biochemical features in CS patients (Leoni et al., submitted). These findings suggest that the *Hras*$^{G12S/+}$ mouse model does not fully recapitulate the metabolic features characterizing the human disease.

Associated with an altered glucose metabolism, we observed a significant increase of autophagy in CS-derived cells, in the steady state condition. The autophagic flux is normally activated when availability of carbon sources is not sufficient to maintain the rate of protein synthesis or provide the required amount of ATP to sustain the metabolic reactions. On the other hand, autophagy functions as a cellular homeostasis system to remove protein aggregates, favor proper organelle turnover, and remove intracellular pathogens (65). In this context, we hypothesize that the high production of oxidant species, including $O_2^{\bullet-}$, H_2O_2, $^{\bullet}OH$ and $ONOO^-$, observed in patients' cells, which represents a toxic class of molecules highly reactive towards lipids, proteins and DNA (66-

68), accelerate the autophagic flux via AMPK activation to concomitantly reduce ROS/RNS concentration and the resulting oxidated biomolecules and organelles (51). According to this model, accelerated autophagy as a basal cellular catabolic process is suggested to represent a cellular process contributing to the increased resting energy expenditure observed in CS patients.

In physiological conditions, the main radical species produced in tissues are $O2^{\bullet}$ and $NO^{\bullet}$. These radicals participate to cell signaling through the direct or indirect (*i.e.*, via H_2O_2) reversible-redox modification of critical thiols located within catalytic enzymes or regulatory sites, as well as in receptors, channels and transporters, transcription factors, kinases, and phosphatases (69). Multiple lines of evidence support the view that RAS signaling is able to regulate the production of redox agents, and that these species, in turn, can function as effector molecules modulating multiple signaling pathways and cellular processes (29-31,70,71). Based on these considerations, the present findings suggest that the aberrant increase of reactive oxidizing species in cells with disease-causing *HRAS* mutations is the unifying event promoting dysregulated glucose metabolism and accelerated autophagy. Specifically, it has been demonstrated that RAS signaling activation promote the NADPH oxidase activation and that the $HRAS^{V12}$ mutant positively regulates the NADPH oxidase system NOXO4-$p22^{phox}$ with consequent hyper production of ROS (32). Consistent with our findings, an increase of ROS levels in CS had previously been reported (72), even though it was tentatively linked to the occurrence of an increased oxidative stress in cells and augmented neoplastic risk associated with this condition. In that work, CS patients had been treated with an antioxidant therapy (*i.e.*, potassium ascorbate with ribose), reporting positive effects in terms of oxidative stress reduction and an apparent improvement of clinical features (*e.g.*, psychomotor development and evolution of heart diseases) (73). Treatment of patients' fibroblasts with antioxidants (*i.e.*, ascorbic acid and N-acetylcysteine), however, did not result in any significant change in ROS level (data not shown). As shown in this work, we suggest an alternative strategy directed to treat cells with wortmannin, a drug targeting both p38 and the PI3K complexes, was able

to counterbalance the two main process altered in CS cells, resulting in a reduced level of glucose intake with consequent lipid droplets consumption, and autophagy inhibition.

Even though life expectancy of patients with CS has increased in the last years due to a better understanding of the natural history of disease, an improvement of patients' care and a more effective prevention of comorbidities, the aspects related to the bioenergetic alterations characterizing this disorder still need to be fully understood. The present findings provide a link between HRAS functional upregulation and metabolic dysfunction observed in fibroblasts from patients with CS, and identify p38 and PI3K signaling as putative targets to revert the metabolic dysfunction occurring in these cells.

Materials and Methods

The study was approved by the local Istitutional Ethical Committees of the *Università Cattolica del Sacro Cuore*/*Fondazione Policlinico Universitario Agostino Gemelli* IRCCS, and Ospedale Pediatrico Bambino Gesù IRCCS.

Cell Cultures

Skin fibroblasts isolated from skin biopsy (subjects CS and age-matched healthy donors) were cultured in Dulbecco's modified Eagle's medium (Gibco) supplemented with 10 % heat-inactivated fetal bovine serum (Gibco) and 1 % penicillin-streptomycin, at 37 °C with 5% CO_2. Diagnosis was molecularly confirmed in all cases, who were heterozygous for de novo missense changes involving Gly12 (p.Gly12Ser; P1, P3, P5, P6, P7, P8 and P9) and Gly13 (p.Gly13Ser; P2 and P4) residues. As patients' fibroblasts are characterized by a senescent phenotype at late passages, all experiments were performed using fibroblasts at early passages (P3-P6) only.

Antibodies

The following antibodies were used: rabbit polyclonal anti-GLUT4 antibody (Invitrogen, #23052); goat polyclonal anti-GLUT4 antibody (N-20 Santa Cruz #sc1606); DAPI (Invitrogen, #D1306); Bodipy dye (Thermo Fisher, #D3922); rabbit polyclonal anti-GLUT1 (ABclonal, #A6982); rabbit polyclonal anti p-AKT (Cell Signaling, #9271S); mouse monoclonal p-p38 (Cell Signaling, #9216S); mouse monoclonal p-AMPK (Cell Signaling, #2335S); mouse monoclonal anti-GAPDH (Santa Cruz, #sc32233); rabbit monoclonal anti-LC3I/II antibody (Cell signaling, #12741S).

NMR spectroscopy

Cells grown to 60-70% confluence were trypsinized 24h after culture medium change, counted, and assessed for viability (80-90%) and membrane integrity by trypan blue staining. Cells were washed twice with ice-cold physiological saline solution and pellets resuspended in 0.5 ml of ice-cold twice-distilled water. Aqueous extracts (from 10 x 10^6 cells/sample) were prepared in EtOH 70% according to an established protocol (Iorio et al, 2005). Briefly, samples were ultra-sonicated at 20 kHz by a MSE ultrasonic disintegrator Mk2 (Crawley) and centrifuged at 14000 x g for 30 min. Supernatants were lyophilized twice in a RVT 4104 Savant lyophilizer (Mildford), and the residue resuspended in 0.7 ml D_2O (Sigma-Aldrich, St. Louis, MO, USA) containing 0.1 mM 3-(trimethylsilyl)-propionic-2,2,3,3-d4 acid sodium salt (TSP) as internal standard. High-resolution NMR experiments (25°C) were performed at 9.4T (Bruker AVANCE). ^{1}H-NMR spectra of cell extracts were acquired using 90° flip angle, 30 s repetition time, 32K time domain data points and 128 transients (73,74).

Metabolite extraction

The pellet samples were resuspended by adding 0.10 mL of ice-cold ultra-pure water (18MΩ) to lyse cells. The samples were sonicated 3-5 times for 1 second each time. The tubes were plunged into dry ice at 4 °C for 0.5 min and then into a water bath at 37 °C for 0.5 min. To each tube, 0.6 mL of -20 °C methanol and then 0.4 mL of -20 °C chloroform was added. Tubes were mixed every 5 min for 30 min. Subsequently, 0.10 mL ice-cold pH-adjusted ultra-pure water was added to each

tube, before being transferred to -20 °C for 2-8 h. After thawing, the tubes were centrifuged at 13,500 × g for 10 min at 4 °C and the collected supernatants were dried to obtain visible pellets. Finally, the dried samples were re-suspended in 0.1 mL of water, 5% formic acid and transferred to glass autosampler vials for LC/MS analysis.

Ultra high-performance liquid chromatograph-mass spectrometry (UHPLC-MS) and metabolome data processing

Twenty microliters of supernatants (two technical replicates) were injected into an ultra high-performance liquid chromatography (UHPLC) system (Ultimate 3000, Thermo) coupled to a high-resolution mass spectrometer (Q Exactive, Thermo). Chromatographic separations were achieved by using a Reprosil C18 column (2.0 mm × 150 mm, 2.5 μm; Dr Maisch, Germany) at 30 °C and 0.2 mL/min flow rate. A 0-100% linear gradient of solvent A (ddH2O, 0.1% formic acid) to B (acetonitrile, 0.1% formic acid) was employed over 20 min, returning to 100% A in 2 min and with a 6-min post-time solvent A hold. The MS system operated in positive ion mode and in full-MS scan mode (2 μscans) at 70,000 resolution in the 70 to 800 m/z range, with a target of 1×106 ions and a maximum ion injection time (IT) of 35 ms. Source ionization parameters were: spray voltage, 3.8 kV; capillary temperature, 300 °C; sheath gas, 40; auxiliary gas, 25; S-Lens level, 45. Calibration was performed before each analysis against positive ion mode calibration mixes (Piercenet, Thermo Fisher, Rockford, IL) to ensure sub ppm error of the intact mass.
Raw files of replicates were exported and converted into mzXML format through MassMatrix (Cleveland, OH), then processed by MAVEN.52. MS chromatograms were elaborated for peak alignment, matching and comparison of parent and fragment ions, and tentative metabolite identification (within a 2 ppm mass-deviation range between observed and expected results against the imported KEGG database).

Evaluation of mitochondrial ATP content and Complex V activity

The content of cellular ATP was assayed using the ATPLITE 1 STEP (PerkinElmer) according to the procedure recommended by the manufacturer. Briefly, we have set up a 96-well reading plate seeding 2×10^4 cells. Patient's and control's fibroblasts was grown, either in regular medium as well as in a restrictive GAL medium (glucose-free DMEM, supplemented with 5mM galactose, and 10% dialyzed FBS) for 24h and 48h. Luminescence was measured using the EnSpire Multimode Plate Readers (PerkinElmer, USA) and the data obtained normalized with the protein content. Complex V activity (in the direction of ATP synthesis) was measured in fibroblast mitochondria, using reported spectrophotometric methods (75).

GLUT4 and lipid droplets evaluation by immunofluorescence.

Twenty thousand fibroblasts were seeded on glass coverslip and maintained in culture with complete medium for 24 h. To evaluate the GLUT4 content cells were fixed with PFA 3%, permeabilized with 0.5% Triton X-100 (10 min at room temperature), and then stained with a rabbit polyclonal anti-GLUT4 antibody followed by the appropriate secondary antibody and DAPI for DNA. To assess the PM translocated GLUT4 levels, cells were directly stained with a goat polyclonal anti-GLUT4 antibody (specific for the N-terminal transporter portion) followed by the appropriate secondary antibody, without prior fixation or permeabilization. After staining, cells were fixed with cold methanol and nuclei were stained with DAPI.

Lipid droplets content was evaluated on cells after fixation with PFA 3% and permeabilization with 0.5% Triton X-100 by using Bodipy dye.

Confocal microscopy analyses were performed in three independent series of experiments on a Leica TCS SP2 AOBS apparatus (Leica Microsystems, Wetzlar, Germany) using excitation spectral laser lines at 405, 488 and 594 nm, using the confocal software (Leica) and Photoshop CS5 (Adobe Systems, San Jose, CA, USA). Signals from different fluorescent probes were taken in sequential scanning mode, several fields of view (> 200 cells) were analyzed for each labeling condition, and representative results are shown.

Glucose uptake assay

$1X10^4$ fibroblasts were seeded on 96-well assay plate in DMEM high complete medium in the evening the day before the assay to not permit the cells division. Following medium removal, cells were washed (1× PBS), and 50 µl of 1 mM 2-DG (Glucose Uptake-Glo Assay, Promega) diluted in DMEM without glucose was added and then incubated for 10 minutes. Cells were then lysed and neutralized before a custom lucigenic reaction mixture was added. Luminescence intensity expressed as relative light unit was measured according to the manufacturer's instructions, using a 0.3 integration interval on a VICTOR, Perkin Elmer multi-label plate reader. Glucose uptake was calculated dividing the luminescence values for cells number. To evaluate the wortmannin effect on glucose intake the cells were pre-treated (2 hours) with 500nM wortmannin before measuring the glucose uptake or untreated.

Lipid droplets consumption and regeneration assay

Fibroblast cells were seeded on glass coverslip and allowed to adhere with complete medium. Then, cells were starved for 18 hours using a culture medium without serum (FBS) and glucose. After starvation cell culture was divided in three groups, one was fixed at once with PFA 3% to evaluate lipid droplets consumption. To evaluate lipid droplets regeneration the second group was treated with medium containing glucose (D-MEM high, Gibco) without serum and the third group was treated with medium containing only 10% FBS for 10 minutes, then cells of the two groups were fixed with PFA 3% and permeabilized with 0.5% Triton X-100. Lipid droplets content was evaluated by using Bodipy dye (Thermo Fisher, #D3922) on a Leica TCS SP2 AOBS apparatus. Lipid droplets consumption was evaluated also after treatment with wortmannin (SIGMA) 500nM for two hours, as reported above.

Electron Paramagnetic Resonance (EPR) detection of ROS and RNS levels

The spin probe 1-hydroxy-3-carboxy-pyrrolidine (CPH; ENZO Life Sciences, Farmingdale, NY) was added (0.5 mM final concentration) to 10 x 10^6 cells/ml in phosphate buffer, pH 7.4. After 20

min at 37°C, samples were drawn up into a gas-permeable Teflon tube, and inserted into a quartz tube. EPR spectra were measured in air at 37°C on a Bruker e-Scan (Bruker, Rheinstetten, Germany). The characterization of ROS formed was performed by pre-incubating fibroblasts, for 15 min at 37° C, with the specific scavengers/inhibitors membrane-permeable superoxide dismutase conjugated to Polyethylene Glycol (PEG-Sod; 10 µg/ml), catalase (Cat; 10 µg/ml), or diethylenetriamine pentaacetic acid (DTPA; 1 mM). The involvement of nitric oxide ($^{\bullet}$NO) synthase was evaluated by pre-treating cells for 1h at 37 °C with N-monomethyl-L-arginine (NMA; 5 mM). The oxidation of CPH was monitored by the formation of the characteristic 3-line spectrum with hyperfine coupling constant of 1.63 ± 0.04 mT, attributable to the corresponding nitroxide radical 3-carboxyproxyl (CP$^{\bullet}$). The intensity of CP$^{\bullet}$ was measured as peak-to-peak linewidth and taken as the measure of ROS-mediated CPH oxidation. Spectrometer conditions common to all spectra were: modulation frequency, 100 kHz; microwave frequency, 9.4 GHz; microwave power, 20 mW; gain $1x10^4$; modulation amplitude, 0.1 mT; conversion time, 20.5 ms; time constant, 82 ms; sweep time, 21 s; number of scans, 10.

Western blot assays to evaluate GLUT1, GLUT4, and phosphorylated AKT, AMPK and p38

To evaluate GLUT1/GLUT4 expression level and AKT, p38 and AMPKα phosphorylation levels patients' fibroblasts, cultured in complete medium, were harvested and lysed using a RIPA buffer containing a phosphatase and protease inhibitors cocktail (Promega). For western blot analyses, cell extracts were separated by 10% sodium dodecyl sulfate–polyacrylamide gel electrophoresis and transferred to nitrocellulose membranes (Bio-Rad). Blots were then incubated with the relevant antibodies. Membranes were re-probed with a mouse monoclonal anti-GAPDH to normalize protein content.

Autophagic flux evaluation

Autophagy in patients' fibroblasts were determined evaluating the expression level of LC3I/II proteins, the highly specific autophagosomal marker, in steady state condition of culture as well as

after treatment with Earle balanced salt solution (EBSS; Gibco) for 2, 4, and 8 hours. Inhibition of autophagy degradation was attained by treating cells with 200 nmol/L bafilomycin A1 for 4 hours (SIGMA). To test the wortmannin effect on autophagy the cells were treated with 200 nM wortmannin (SIGMA) both in the steady state condition and together EBSS stimulation, for two hours. After the treatment the cells were harvested and lysed using a RIPA buffer containing a phosphatase and protease inhibitors cocktail (Promega). For all blots, equal amounts of cell lysates were resolved on 10% polyacrylamide gels. Membranes were probed with rabbit monoclonal anti-LC3I/II antibody and with a mouse monoclonal anti-GAPDH antibody (Santa Cruz, sc32233) for normalization.

Lipid extraction and analysis

For each line, cells cultured in 150 cm^2 dishes were harvested using trypsin after reaching confluency, rinsed with phosphate-buffered saline (PBS) and pelleted by centrifugation. Cell pellet was resuspended in 1 ml 0.9% NaCl and 6 ml of chloroform/methanol (2:1, v/v) were added. Mixture was vortexed vigorously and centrifuged at 1500 g for 15 min, aqueous phase was discarded and organic phase was dried under N_2 gas. Lipid extracts from 1.5x106 cells were applied on high-performance thin-layer chromatography (HPTLC) silica gel 60 plates (Merck, Darmstadt, Germany). Neutral lipids were resolved using a solvent system of hexane/diethyl ether/acetic acid (70:30:1, v/v/v) and were detected by staining with an aqueous solution containing 3% cupric acetate and 8% phosphoric acid and subsequent charring at 140 °C for 10 min. Lipids were identified by comigration of commercially available standards and quantified using Alphaview software (Protein Simple, San Jose, CA, USA).

Quantitative Real Time PCR (q-PCR)

Total RNA was extracted by fibroblasts derived from patients and healthy subjects using TRIzol Reagent (Invitrogen). RNA quantity and quality were assessed using a NanoDrop 2000 spectrophotometer (Thermo Scientific). One microgram of each RNA was reverse-transcribed with

SensiFAST cDNA Synthesis Kit (Bioline, London, UK) according to the manufacturer's instructions. Quantitative Real Time PCR (q-PCR) experiments for *GLUT1* mRNA levels were performed using specific TaqMan Real-Time Gene Expression Assays (*GLUT1* Assay ID: Hs00892681_m1 by Applied Biosystems) and the TaqMan Universal Master Mix II, no UNG (Applied Biosystems), following the manufacturer's instructions. Gene expression data were normalized to human *GAPDH* mRNA levels (Assay ID: Hs99999905_m1, Applied Biosystems). All q-PCR experiments were performed on a StepOne Real Time System (Applied Biosystems) machine and relative quantification (mRNA or miRNA) was performed by the Comparative Ct method (76). Each sample was run in triplicate in at least three independent experiments.

Statistics

Statistical significance for mass spectrometry data analysis was performed using a custom script in R vr. 3.5.3. The raw count peak area was compared between control and CS samples for each metabolite using a two-tailed, unpaired and heteroscedastic t-test ($p < 0.05$). To control for false discovery rate (FDR), multiple testing correction was performed at a *q*-value cut-off of 0.1. Values of mass-to-charge ratio (m/z), *p*-value, *q*-value and mean peak area count are reported in Table S1. Statistical significance for NMR data analysis and *GLUT1* mRNA expression level were assessed by Mann-Whitney test, whereas for glucose intake assays were calculated by one-way ANOVA with Tukey's correction for multiple testing. In all other experiments, statistical analysis was performed using paired Student t-test. Results were graphed with Graphpad Prism 5.01 (Graphpad Software Inc.). The statistical significance is denoted on graph by asterisks (*), where *p < 0.05, **p <0.005, ***p < 0.001, and n.s. = not significant.

Acknowledgements

The authors wish to thank the participating patients and their families, and Serenella Venanzi (Istituto Superiore di Sanità, Rome) for technical support. This work has been supported by Italian Ministry

of Health (Ricerca Corrente 2019 and 2020), EJP-RD (NSEuroNet), and AIRC (IG 21614). GC is recipient of an AISC (*Associazione Italiana Sindrome Costello e cardiofaciocutanea*) research fellowship.

Conflict of Interest Statement

The authors declare that they do not have any conflict of interest.

References

1. Colicelli, J. (2004) Human RAS superfamily proteins and related GTPases. *Sci. STKE*, **7**,250:RE13.
2. Karnoub , A.E. and Weinberg, R.A. (2008) Ras oncogenes: split personalities**.** *Nat. Rev. Mol. Cell Biol*., **9**,517-531.
3. Li, S., Balmain A. and Counter, C.M. (2018) A model for RAS mutation patterns in cancers: finding the sweet spot. *Nat. Rev. Cancer*, **18**,767-777.
4. Aoki, Y., Niihori, T., Kawame, H., Kurosawa, K., Ohashi, H., Tanaka, Y., Filocamo, M., Kato, K., Suzuki, Y., Kure, S. et al. (2005) Germline mutations in HRAS proto-oncogene cause Costello syndrome. *Nat. Genet*., **37**,1038-1040.
5. Zampino, G., Pantaleoni, F., Carta, C., Cobellis, G., Vasta, I., Neri, C., A Pogna, E., De Feo, E., Delogu, A., Sarkozy, A. et al. (2007) Diversity, parental germline origin, and phenotypic spectrum of de novo HRAS missense changes in Costello syndrome. *Hum. Mutat*., **28**,265-272.
6. Gripp, K.W., A Morse, L., Axelrad, M., Chatfield, K.C., Chidekel , A., Dobyns, W., Doyle, D., Kerr, B., E Lin, A., Schwartz, D.D. et al. (2019) Costello syndrome: Clinical phenotype, genotype, and management guidelines. *Am. J. Med. Genet. A.*, **179**,1725-1744.
7. Gregersen, N. & Viljoen, D. (2004) Costello syndrome with growth hormone deficiency and hypoglycemia: a new report and review of the endocrine associations. *Am. J. Med. Genet. A.*, **129A**,171-175.
8. Stein, R.I., Legault, L., Daneman, D., Weksberg, R. and Hamilton, J. (2004) Growth hormone deficiency in Costello syndrome. *Am. J. Med. Genet. A.*, **129A**,166-170.
9. Leoni, C. & Flex, E. (2018) Costello Syndrome: The Challenge of Hypoglycemia and Failure to Thrive. *EBioMedicine*, **27**,5-6.

10. Leoni, C., Onesimo, R., Giorgio, V., Diamanti, A., Giorgio, D., Martini, L., Rossodivita, A., Tartaglia, M. and Zampino G. (2016) Understanding Growth Failure in Costello Syndrome: Increased Resting Energy Expenditure. *J Pediatr*., **170**,322-324.
11. Leoni, C., Giorgio, V., Onesimo, R., Kuczynska, E. and Zampino, G. (2020) Impact of Costello syndrome on growth patterns. *Am. J. Med. Genet. A.*, **182**,2797-2799.
12. Ambrosini G., Dalla Pozza, E., Fanelli, G., Di Carlo, C., Vettori, A., Cannino , G., Cavallini, C., Carmona-Carmona, C. A., Brandi, J., Rinalducci S. et al. (2020) Progressively De-Differentiated Pancreatic Cancer Cells Shift from Glycolysis to Oxidative Metabolism and Gain a Quiescent Stem State. Cells, **9**,1572.
13. Iorio, E., Ricci, A., Pisanu, M.E., Bagnoli, M., Podo, F. and Canevari S. (2013) Choline metabolic profiling by magnetic resonance spectroscopy. *Methods Mol. Biol*., **1049**,255-270.
14. Canese, R., Iorio, E., Ricci, A., Pisanu, M.E., Giannini, M. and Podo, F.(2009) Metabolite quantification in tumours by magnetic resonance spectroscopy: objectives, results and perspectives. *Current medical imaging reviews* **5**,110.
15. Hu, Y., Lu, W., Chen, G., Wang, P., Chen, Z., Zhou, Y., Ogasawara, M., Trachootham, D., Feng, L., Pelicano H. et al. (2012) K-ras (G12V) transformation leads to mitochondrial dysfunction and a metabolic switch from oxidative phosphorylation to glycolysis. *Cell Res*., **22**,399-412.
16. DeBerardinis R.J., Lum, J.J., Hatzivassiliou, G. and Thompson, C.B. (2008) The biology of cancer: metabolic reprogramming fuels cell growth and proliferation. *Cell Metab*., 7,11-20.
17. Warburg, O. (1956) On the origin of cancer cells. *Science*, **123**,309-314.
18. Vander Heiden, M.G., Cantley, L.C. and Thompson, C.B. (2009) Understanding the Warburg effect: the metabolic requirements of cell proliferation. *Science*, **324**,1029-1033.
19. Gillies, R.J., Robey, I. and Gatenby, R.A. (2008) Causes and consequences of increased glucose metabolism of cancers. *J. Nucl. Med.*, 49 Suppl **2**:24S-42S.

20. Kroemer, G. & Pouyssegur, J. (2008) Tumor cell metabolism: cancer's Achilles' heel. *Cancer Cell*, **13**,472-482.

21. Bryant, N.J., Govers, R. and James, D.E. (2002) Regulated transport of the glucose transporter GLUT4. *Nat. Rev. Mol. Cell Biol.*, **3**,267-277.

22. Govers, R. , Coster, A.C.F. and James, D.E. (2004) Insulin increases cell surface GLUT4 levels by dose dependently discharging GLUT4 into a cell surface recycling pathway. *Mol. Cell Biol.*, **24**,6456-6466.

23. Rosenberger, G., Meien, S. and Kutsche, K. (2009) Oncogenic HRAS mutations cause prolonged PI3K signaling in response to epidermal growth factor in fibroblasts of patients with Costello syndrome. *Hum Mutat.*, **30**,352-362.

24. Gatenby, R.A. & Gillies R.J. (2004) Why do cancers have high aerobic glycolysis? *Nat. Rev. Cancer*, **4**,891-899.

25. Longo, N. , Bell, G.I., Shuster, R.C., Griffin, L.D., Langley, S.D. and Elsas, L.J. (1990) Human fibroblasts express the insulin-responsive glucose transporter (GLUT4). *Trans. Assoc. Am. Physicians*, **103**,202-213.

26. Yamaguchi, S., Katahira, H., Ozawa, S., Nakamichi, Y., Tanaka, T., Shimoyama, T., Takahashi, K., Yoshimoto, K., Imaizumi, M.O., Nagamatsu, S. et al. (2005) Activators of AMP-activated protein kinase enhance GLUT4 translocation and its glucose transport activity in 3T3-L1 adipocytes. *Am. J. Physiol. Endocrinol. Metab.*, **289**,E643-649.

27. Lemieux, K., Konrad, D., Klip, A. and Marette, A. (2003) The AMP-activated protein kinase activator AICAR does not induce GLUT4 translocation to transverse tubules but stimulates glucose uptake and p38 mitogen-activated protein kinases alpha and beta in skeletal muscle. *FASEB J.*, **17**,1658-1665.

28. Bazuine , M.,Ouwens, D.M., Gomes de Mesquita, D.S. and Maassen, J.A. (2003) Arsenite stimulated glucose transport in 3T3-L1 adipocytes involves both Glut4 translocation and p38 MAPK activity. *Eur. J. Biochem.*, **270**,3891-3903.

29. Irani, K., Xia, Y., Zweier, J.L., Sollott, S.J., Der, C.J., Fearon, E.R., Sundaresan, M., Finkel, T. and Goldschmidt-Clermont, P.J. (1997) Mitogenic signaling mediated by oxidants in Ras-transformed fibroblasts. *Science*, **275**,1649-1652.

30. Mitsushita, J., Lambeth, J.D. and Kamata, T. (2004) The superoxide-generating oxidase Nox1 is functionally required for Ras oncogene transformation. *Cancer Res*., **64**,3580-3585.

31. Brown, D.I. & Griendling, K.K. (2009) Nox proteins in signal transduction. *Free Radic*. *Biol*. *Med*., **47**,1239-1253.

32. Weyemi, U., Lagente-Chevallier, O., Boufraqech, M., Prenois, F., Courtin, F., Caillou, B., Talbot, M., Dardalhon, M., Al Ghuzlan, A., Bidart, J-M. et al. (2012) ROS-generating NADPH oxidase NOX4 is a critical mediator in oncogenic H-Ras-induced DNA damage and subsequent senescence. *Oncogene*, **31**,1117-1129.

33. Zmijewski, J.W., Banerjee, S., Bae, H., Friggeri, A., Lazarowski, E.R. and Abraham E. (2010) Exposure to hydrogen peroxide induces oxidation and activation of AMP-activated protein kinase. *J. Biol*. *Chem*., **285**,33154-33164.

34. Shao , D., Oka, S-I., Liu, T., Zhai, P., Ago, T., Sciarretta, S., Li, H. and Sadoshima, J. (2014) A redox-dependent mechanism for regulation of AMPK activation by Thioredoxin1 during energy starvation. *Cell Metab*., **19**,232-245.

35. Hinchy, E.C., Gruszczyk, A.V., Willows, R., Navaratnam, N., Hall, N.R., Bates, G., Bright, T.P., Krieg, T., Carling, D. and Murphy M.P. (2018) Mitochondria-derived ROS activate AMP-activated protein kinase (AMPK) indirectly. *J. Biol*. *Chem*. **293**,17208-17217.

36. Son, Y., Cheong, Y-K., Kim, N.H., Chung, H-T., Kang, D.G. and Pae H-O. (2011) Mitogen-Activated Protein Kinases and Reactive Oxygen Species: How Can ROS Activate MAPK Pathways? *J. Signal Transduct.* **2011**,792639.

37. Jia, Y.T., Wei, W., Ma, B., Xu, Y., Liu, W-J., Wang, Y., Lv, K-Y., Tang, H-T., Wei, D. and Xia Z-F. (2007) Activation of p38 MAPK by reactive oxygen species is essential in a rat model of stress-induced gastric mucosal injury. *J. Immunol*., **179**,7808-7819.

38. McCubrey, J.A., Lahair, M.M. and Franklin, R.A. (2006) Reactive oxygen species-induced activation of the MAP kinase signaling pathways. *Antioxid. Redox Signal.*, **8**,1775-1789.

39. Dikalov, S.I., Kirilyuk, I.A., Voinov, M. and Grigor'ev, I.A. (2011) EPR detection of cellular and mitochondrial superoxide using cyclic hydroxylamines. *Free Radic. Res.*, **45**,417-430.

40. Liu, X., Xu, X., Shang, R. and Chen, Y. (2018) Asymmetric dimethylarginine (ADMA) as an important risk factor for the increased cardiovascular diseases and heart failure in chronic kidney disease. *Nitric Oxide*, **78**,113-120.

41. Kumar, S., Sun, X., Noonepalle, S. K., Lu, Q., Zemskov, E., Wang, T., Aggarwal, S., Gross, C., Sharma, S., Desai A.A. et al. (2017) Hyper-activation of pp60Src limits nitric oxide signaling by increasing asymmetric dimethylarginine levels during acute lung injury. *Free Radic. Biol. Med.*, **102**,217-228.

42. Schmidt, H.M., Kelley, E.E. and Straub, A.C. (2019) The impact of xanthine oxidase (XO) on hemolytic diseases. Redox Biol., **21**,101072.

43. Kaur, H. & Halliwell, B. (1990) Action of biologically-relevant oxidizing species upon uric acid. Identification of uric acid oxidation product. Chem. Biol. Interact., **73**,235-247.

44. Mieyal, J.J. & Chock, P.B. (2012) Posttranslational modification of cysteine in redox signaling and oxidative stress: Focus on s-glutathionylation. Antioxid. Redox Signal., **16**,471-475.

45. Berardi, M.J. & Fantin, V.R. (2011) Survival of the fittest: metabolic adaptations in cancer. *Curr. Opin. Genet. Dev.*, **21**,59-66.

46. Menendez, J.A. & Lupu, R. (2007) Fatty acid synthase and the lipogenic phenotype in cancer pathogenesis. *Nat. Rev. Cancer*, **7**,763-777.

47. Hardie, D.G., Ross, F.A. and Hawley, S.A. (2012) AMPK: a nutrient and energy sensor that maintains energy homeostasis. *Nat. Rev. Mol. Cell Biol.*, **13**,251-262.

48. Kim, J., Kundu, M., Viollet, B. and Guan, K.L. (2011) AMPK and mTOR regulate autophagy through direct phosphorylation of Ulk1. Nat Cell Biol. **13**,132-141.

49. Mihaylova, M.M. & Shaw, R.J. (2011) The AMPK signalling pathway coordinates cell growth, autophagy and metabolism. *Nat. Cell Biol.*, **13**,1016-1023.

50. Filomeni, G., De Zio, D. and Cecconi, F. (2015) Oxidative stress and autophagy: the clash between damage and metabolic needs. *Cell Death Differ.*, **22**,377-388.

51. Carling, D., Mayer, F.V., Sanders, M.J. and Gamblin, S.J. (2011) AMP-activated protein kinase: nature's energy sensor. *Nat. Chem. Biol.*, **18**,512-518.

52. Carling, D. & Viollet, B. (2015) Beyond energy homeostasis: the expanding role of AMP-activated protein kinase in regulating metabolism. *Cell Metab.*, **21**,99-104.

53. Somwar, R., Niu, W., Kim, D.Y., Sweeney, G., Randhawa, V.K., Huang, C., Ramlal, T. and Klip, A. (2001) Differential effects of phosphatidylinositol 3-kinase inhibition on intracellular signals regulating GLUT4 translocation and glucose transport. J. Biol. Chem., **276**,46079-46087.

54. Racker, E., Resnick, R.J. and Feldman, R. (1985) Glycolysis and methylaminoisobutyrate uptake in rat-1 cells transfected with ras or myc oncogenes. *Proc. Natl. Acad. Sci U S A*, **82**,3535-3538.

55. Ying, H., Kimmelman, A.C., Lyssiotis, C.A., Hua, S., Chu, G.C., Fletcher-Sananikone, E., Locasale, J.W., Son, J., Zhang, H., Coloff, J.L. et al. (2012) Oncogenic Kras maintains pancreatic tumors through regulation of anabolic glucose metabolism. *Cell*, **149**,656-670.

56. Dard, L., Bellance, N., Lacombe, D. and Rossignol, R. (2018) RAS signalling in energy metabolism and rare human diseases. *Biochim. Biophys. Acta Bioenerg.*, **1859**,845-867.

57. Tanner, L.B., Goglia, A.G., Wei, MH., Sehgal, T., Parsons, L.R., Park, J.O., White, E., Toettcher, J.E. and Rabinowitz J.D. (2018).Four key steps control glycolytic flux in mammalian cells. *Cell Syst.*, **7**,49-62.e8.

58. Gaglio, D., Metallo, C.M., Gameiro, P.A., Hiller, K., Danna, L.S., Balestrieri, C., Alberghina, L., Stephanopoulos, G. and Chiaradonna, F. (2011) Oncogenic K-Ras decouples glucose and glutamine metabolism to support cancer cell growth. *Mol. Syst. Biol.*, **7**,523.

59. Amendola, C.R., Mahaffey, J.P., Parker, S.J., Ahearn, I.M., Chen, W.C., Zhou, M., Court, H., Shi, J., Mendoza, S.L., Morten, M.J. et al. (2019) KRAS4A directly regulates hexokinase 1. *Nature*, **576**,482-486.

60. Dodson, M., Darley-Usmar, V. and Zhang, J. (2013) Cellular metabolic and autophagic pathways: traffic control by redox signaling. *Free Radic. Biol. Med.*, **63**,207-221.

61. De Santis, M.C., Porporato, P.E., Martini, M. and Morandi, A. (2018) Signaling Pathways Regulating Redox Balance in Cancer Metabolism. *Front. Oncol.*, **8**,126.

62. Hatzivassiliou, G., Zhao, F., Bauer, D.E., Andreadis, C., Shaw, A.N., Dhanak, D., Hingorani, S. R., Tuveson, D.A. and Thompson, C.B. (2005) ATP citrate lyase inhibition can suppress tumor cell growth. *Cancer Cell*, **8**,311-321.

63. Currie, E., Schulze, A., Zechner, R., Walther, T.C and Farese Jr, R.V. (2013) Cellular fatty acid metabolism and cancer. *Cell Metab.*, **18**,153-161.

64. Oba, D., Inoue, S., Miyagawa-Tomita, S., Nakashima, Y., Niihori, T., Yamaguchi, S., Matsubara, Y., Aoki, Y. (2016) Mice with an oncogenic HRAS mutation are resistant to high-fat diet-induced obesity and exhibit impaired hepatic energy homeostasis, *EBioMedicine*, **27**,138-150.

65. Anding, A.L. & Baehrecke, E.H. (2017) Cleaning House: Selective Autophagy of Organelles. *Dev. Cell* **41**,10-22.

66. Davies, K. J. (1987) Protein damage and degradation by oxygen radicals. I. general aspects. J. Biol. Chem., **262**,9895–9901.

67. Halliwell, B. (1978) Biochemical mechanisms accounting for the toxic action of oxygen on living organisms: the key role of superoxide dismutase. *Cell Biol. Int. Rep.*, **2**,113-128.

68. Imlay, J.A. & Linn, S. (1988) DNA damage and oxygen radical toxicity. *Science*, **240**,1302-1309.

69. Janssen-Heininger, Y.M.W., Mossman, B.T., Heintz, N.H., Forman, H.J., Kalyanaraman, B., Finkel, T., Stamler, J.S., Rhee, S.G. and van der Vliet, A. (2008) Redox-based regulation of signal transduction: principles, pitfalls, and promises**.** *Free Radic. Biol. Med.*, **45**,1-17.

70. Finkel, T. (2006) Intracellular redox regulation by the family of small GTPases. *Antioxid. Redox Signal.*, **8**,1857-1863.

71. Ferro, E., Goitre, L., Retta, S.F. and Trabalzini, L. (2012) The Interplay between ROS and Ras GTPases: Physiological and Pathological Implications. *J. Signal Transduct.*, **2012**,365769.

72. Anichini, C., Lotti, F., Pietrini, A., Lo Rizzo, C., Longini, M., Proietti, F., Felici, C. and Buonocore, G. (2013) Antioxidant effects of potassium ascorbate with ribose in costello syndrome. *Anticancer Res.*, **33**,691-695.

73. Iorio, E., Mezzanzanica, D., Alberti, P., Spadaro, F., Ramoni, C., D'Ascenzo, S., Millimaggi, D., Pavan, A., Dolo, V. and Canevari, S. et al. (2005) Alterations of choline phospholipid metabolism in ovarian tumor progression. *Cancer Res.*, **65**,9369-9376.

74. Iorio, E., Ricci, A., Bagnoli, M., Pisanu, M. E., Castellano, G., Di Vito, M., Venturini, E., Glunde, K., Bhujwalla, Z. M. and Mezzanzanica, D. et al. (2010) Activation of phosphatidylcholine cycle enzymes in human epithelial ovarian cancer cells. Cancer Res., **70**,2126-2135.

75. Rizza, T., Vazquez-Memije, M.E., Meschini, M.C., Bianchi, M., Tozzi, G., Nesti, C., Piemonte, F., Bertini, E., Santorelli, F.M. and Carrozzo, R. (2009) Assaying ATP synthesis in cultured cells: a valuable tool for the diagnosis of patients with mitochondrial disorders. *Biochem. Biophys. Res. Commun.*, **383**,58-62.

76. Livak, K.J. and Schmittgen, T.D. (2001) Analysis of relative gene expression data using real-time quantitative PCR and the 2(-Delta Delta C(T)) *Method. Methods*, **25**,402-408.

Legends to Figures

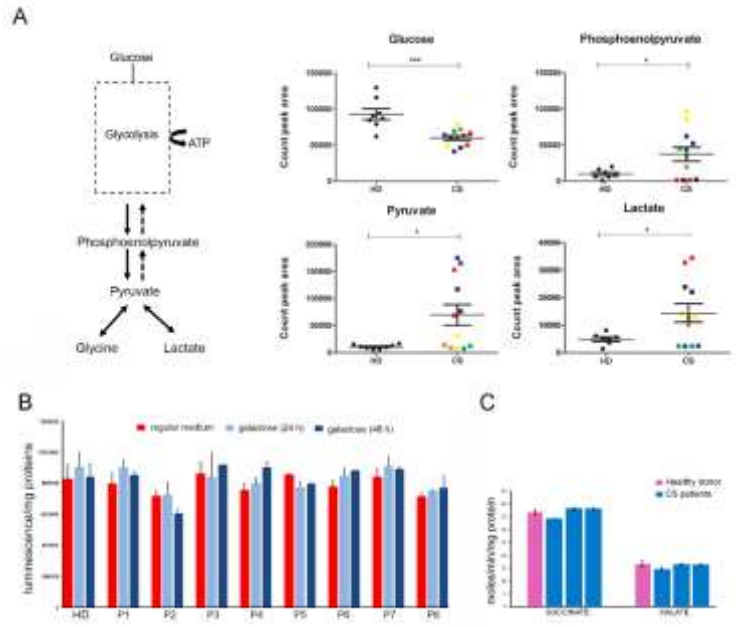

Figure 1. Fibroblasts of patients with Costello syndrome show an accelerated glycolytic flux, which is not associated with defective mitochondrial oxidative phosphorylation activity.

(A) Schematic representation of glucose/pyruvate metabolism (left). Pyruvate, the end product of glycolysis, is generated from phosphoenolpyruvate by pyruvate kinase, and can be converted to lactate by lactate dehydrogenase or glycine *via* a serine intermediate. Scatter graphs show the levels of glucose, phosphoenolpyruvate, pyruvate and lactate in patients (CS, n=6) and healthy donors (HD, n=4) (right) identified by mass spectrometry analysis. Individual values (two technical replicates) and means are shown. Ion count peak area was used to determine metabolite relative abundance. Asterisks indicate statistically significant differences, as assessed by t-test (*$p < 0.05$, ***$p < 0.001$). **(B)** Mitochondrial activity assessment. ATP content was assessed by luminometric assay in control (HD) and patients (CS) fibroblasts cultured either in regular medium or in medium supplemented with galactose. Values referring to the patients are the mean of three independent experiments ± SD, values referring to controls represent the mean of three different control lines, each analyzed 3 times (paired Student t-test). **(C)** Spectrophotometric determination of complex V activity on mitochondria derived from control (HD) and patients (CS) fibroblasts, using succinate or malate as substrate. Means and SD are as above.

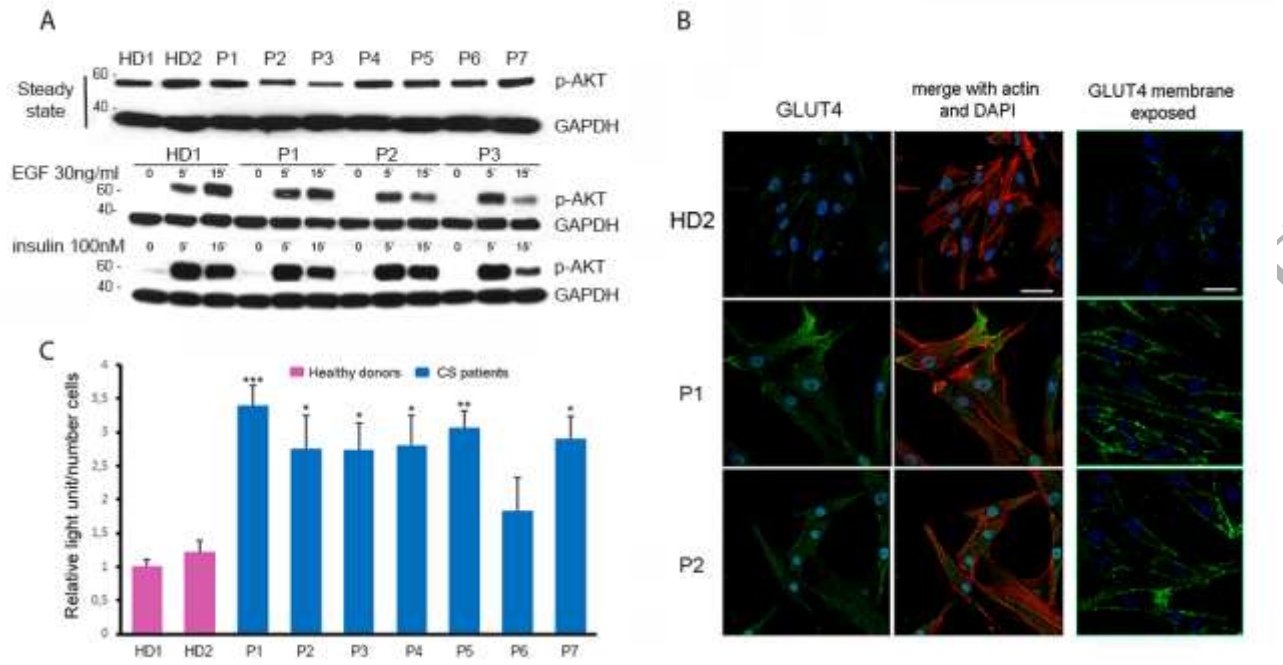

Figure 2. Costello syndrome fibroblasts show a variably enhanced 2DG-glucose uptake basally, which does not depend on PI3K/AKT signaling and is associated to an enhanced translocation of GLUT4 to the plasma membrane.

(A) AKT phosphorylation assay. WB analyses show comparable pAKT levels in fibroblasts from healthy donors (HD) and patients (CS), basally and after EGF (30ng/ml) or insulin (100nM) stimulation. Equal amounts of cell lysates were resolved by 10% polyacrylamide gel electrophoresis. Membranes were probed with an anti-pAKT antibody and then re-probed with an anti-GAPDH antibody for data normalization. **(B)** Confocal laser scanning microscopy analysis documents an increased amount and enhanced plasma membrane translocation of GLUT4 in patients' fibroblasts (CS) compared to control cells (HD). Fixed cells were stained with an anti-GLUT4 rabbit polyclonal antibody followed by goat anti-rabbit Alexa Fluor-488 (green, left panels), whereas not permeabilized cells (right panels) were incubated with an anti-GLUT4 goat monoclonal antibody followed by donkey anti goat Alexa Fluor-488 (green) to stain exposed GLUT4 molecules. Nuclei are visualized by DAPI staining (blue). Scale bars represent 48 μm.

(C) Glucose intake assay. Patients' fibroblasts (CS) show an increase of basal 2DG-glucose uptake compared to controls cells (HD1). The reported values are means ± SEM of three independent

experiments; *p* values were calculated by one-way ANOVA with Tukey's correction for multiple testing (*$p < 0.05$; **$p < 0.005$ ***$p < 0.001$).

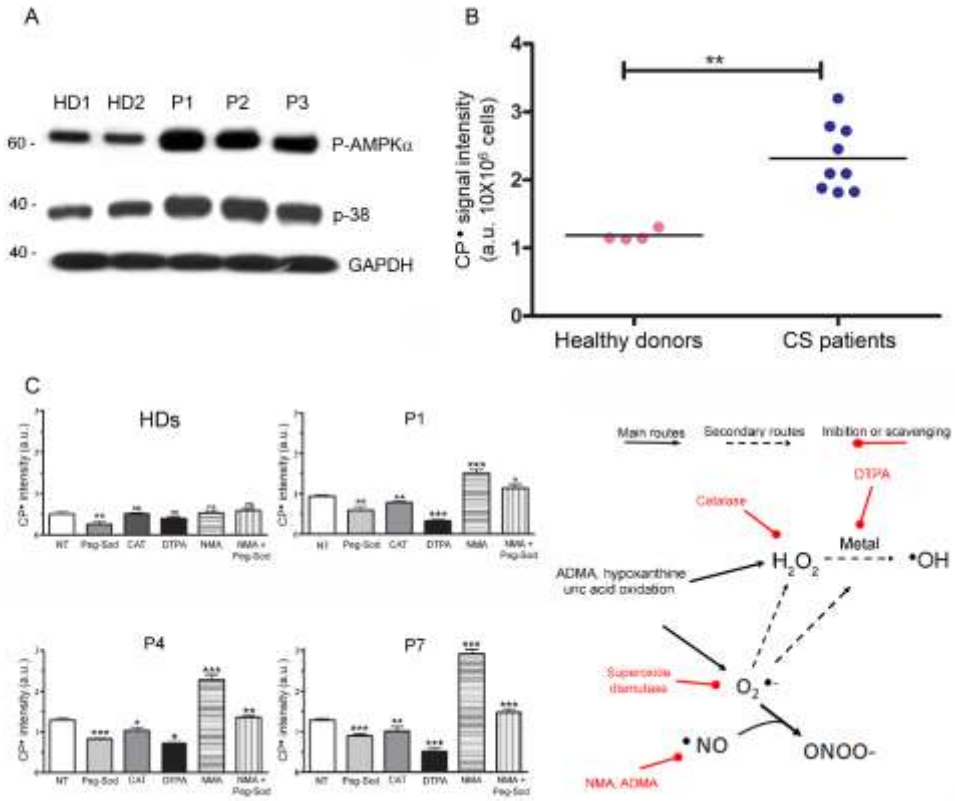

Figure 3. Fibroblasts from patients with Costello syndrome have high reactive oxidizing species levels and show increased AMPK and p38 phosphorylation.

(A) AMPK and p38 phosphorylation assays. AMPK and p38 phosphorylation is enhanced in primary fibroblasts from patients (CS) compared to control cells (HD) cultured in steady state condition. Representative blot of three independent experiments is shown. Equal amount of cell lysates was resolved by 10% polyacrylamide gel electrophoresis. Membranes were probed with anti-phospho-AMPKα and anti-phospho-p38 antibodies and signals were normalized using GAPDH as internal control. **(B)** 3-carboxyproxyl ($CP^{\bullet}$) production assay. ROS-dependent CPH to $CP^{\bullet}$ oxidation was measured in primary fibroblasts ($10x10^6$ cells/ml) from healthy donors (HD) and patients (CS) suspended in PBS, pH 7.4 and treated with 0.5 mM CPH for 10 min at 37 °C. Spectra were acquired by EPR spectrometry and the relative intensity of $CP^{\bullet}$ was expressed as arbitrary units (a.u.) normalized to the cell number. Values are the mean of three independent experiments ± SD (**$p <$

0.005; paired Student t-test). **(C)** EPR competition experiments using different scavengers and inhibitors were performed to characterized the produced ROS and RNS in fibroblasts from patients with Costello syndrome (left). Primary fibroblasts ($10x10^6$ cells/ml) from healthy donors (HD) and patients (P1, P4 and P7) were suspended in PBS, pH 7.4, and pre-incubated for 15 min at 37 °C with 10 µg/ml superoxide dismutase conjugated to polyethylene glycol (PEG-SOD; suitable scavengers of O2•), 10 µg/ml catalase (CAT; suitable scavengers of H_2O_2), 1 mM diethylenetriamine penta-acetic acid, (DTPA; a chelator of transition metals), 5 mM N-monomethyl-l-arginine (NMA; a suitable inhibitor of the NO generating enzyme nitric oxide synthase). Cat and DTPA are cell-impermeable compounds, while PEG-Sod can bind to phospholipid membranes and be taken up by endocytosis. Samples were then treated with 0.5 mM CPH for 10 min at 37 °C. NT indicate samples that were not treated with scavengers or inhibitors. Spectra were acquired by EPR spectrometry and the relative intensity of CP• was expressed as arbitrary units (a.u.) normalized to the cell number. Values referring to patients are the mean of three independent experiments ± SD, whereas those referring to controls represent the mean of three different control lines, each analyzed 3 times (**p* <0.05, ***p* <0.005; ***p>0.001; paired Student t-test).

A scheme of the oxidant species formed in fibroblasts from patients with Costello syndrome is also shown (right). In control fibroblasts, the intensity of CP• was significantly inhibited only in the presence of PEG-SOD, suggesting that O2• is the major radical species produced in these cells. In CS fibroblasts, in addition to PEG-SOD, the intensity of CP• is inhibited also in the presence of CAT and DTPA, indicating that O2• and H_2O_2 are involved in a metal-dependent boosting of Fenton-like reactions producing the strong oxidant hydroxyl radical (•OH). Moreover, in these cells the intensity of CP• is strongly increased by incubation with NMA, suggesting that the inhibition of NO synthesis mediated by NMA allow other oxidants to be more available and reactive towards CPH, favoring its oxidation to CP•. This oxidant is reasonably O_2• or the H_2O_2-derived metal-dependent OH, as the intensity of CP• is comparable to that measured in untreated (NT) fibroblasts from patients when cells were simultaneously pre-incubated with NMA and PEG-SOD. In fibroblasts from patients it is

conceivable to hypothesize the production of peroxynitrite (ONOO-), resulting from the fast reaction between $O_2^{\bullet}$ and NO.

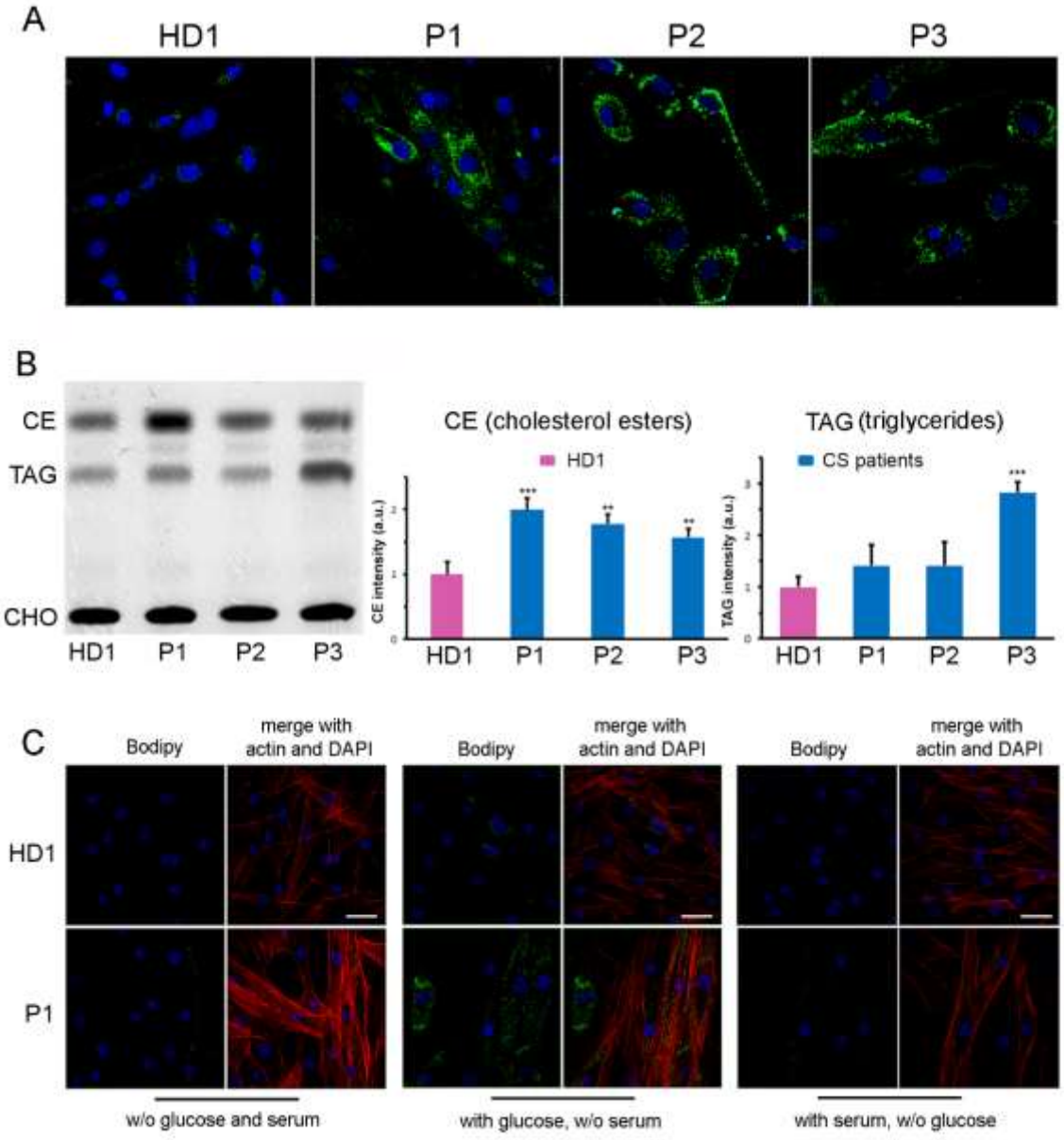

Figure 4. Increased glucose uptake promotes fatty acid synthesis and intracellular storage as lipid droplets in primary fibroblasts from patients with Costello syndrome.

(A) Confocal laser scanning microscopy (CLSM) analysis shows an increased amount of lipid droplets in CS fibroblasts (P1 to P3) compared to control cells (HD1) in the steady state condition. Lipid droplets content was evaluated after fixation with 3% PFA and permeabilization with 0.5%

Triton X-100 by using Bodipy dye (green). Nuclei are visualized by DAPI staining (blue). Scale bar is 48 µm. **(B)** High-performance thin-layer chromatography shows variable higher cholesterol esters (CE) and triglycerides (TAG) levels in CS fibroblasts compared to healthy donor cells. The relative CE and TAG intensities were expressed as arbitrary units (a.u.) normalized to the cell number. The corresponding graphs show the mean +/- SD of 3 independent experiments (**$p < 0.005$ ***$p<0.001$ by paired Student t-test). Data are shown as nmol of metabolites normalized to cell number, asterisks indicate statistically significant differences, as assessed by Mann–Whitney U test (**$p < 0.01$). **(C)** CLSM observations show a direct link between glucose uptake and lipid droplets generation. Cells were starved 18 hours with medium W/O glucose and serum and then treated with medium containing only glucose or only serum for 10 minutes. Panels show that the lipid droplets regenerate significantly only after adding glucose in the medium. Fixed cells were stained with Bodipy dye (green) and an anti-phalloidin antibody conjugated to red-fluorescent Alexa Fluor 633 dye (red). Nuclei are visualized by DAPI staining (blue). Scale bar is 48 µm.

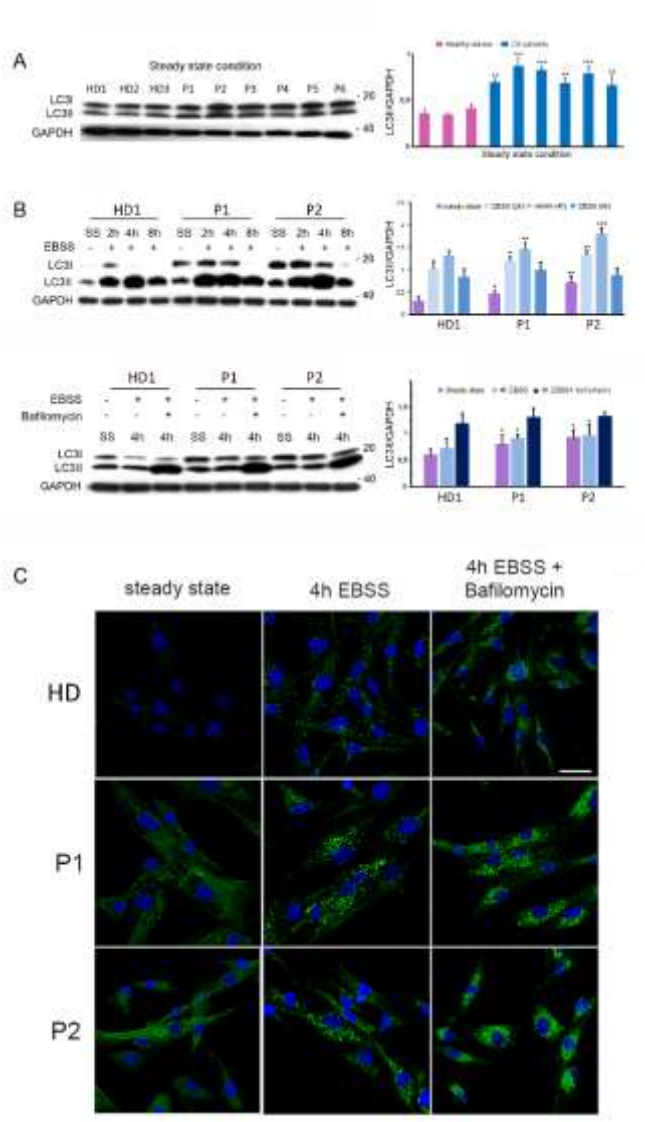

Figure 5. Enhanced autophagic flux induction occurs in fibroblasts from patients with Costello syndrome.

(A) WB analyses performed on patients' fibroblasts show a significant increase of LC3I/II level already in the steady state condition (left). The corresponding graph (right) shows means +/- SD of 3 separate experiments (**$p < 0.005$ ***$p < 0.001$, paired Student t-test). **(B)** LC3II level is further increased after cell incubation with Earle balanced salt solution (EBSS) (above) and treatment with Bafilomycin (200 nM, 4 h) (below), indicating an acceleration of the autophagic flux in cells. The corresponding graphs show means +/- SD of 3 separate experiments (*$p < 0.05$; **$p < 0.005$ ***$p < 0.001$, paired Student t-test). **(C)** Confocal laser scanner microscopy analysis, performed in the same

experimental conditions reported above (panel B), confirms enhanced autophagy in patients' cells. Fixed cells were stained with rabbit monoclonal anti-LC3I/II antibody followed by rabbit anti goat Alexa Fluor-488 (green). Nuclei are visualized by DAPI staining (blue). Scale bar correspond to 35 µm.

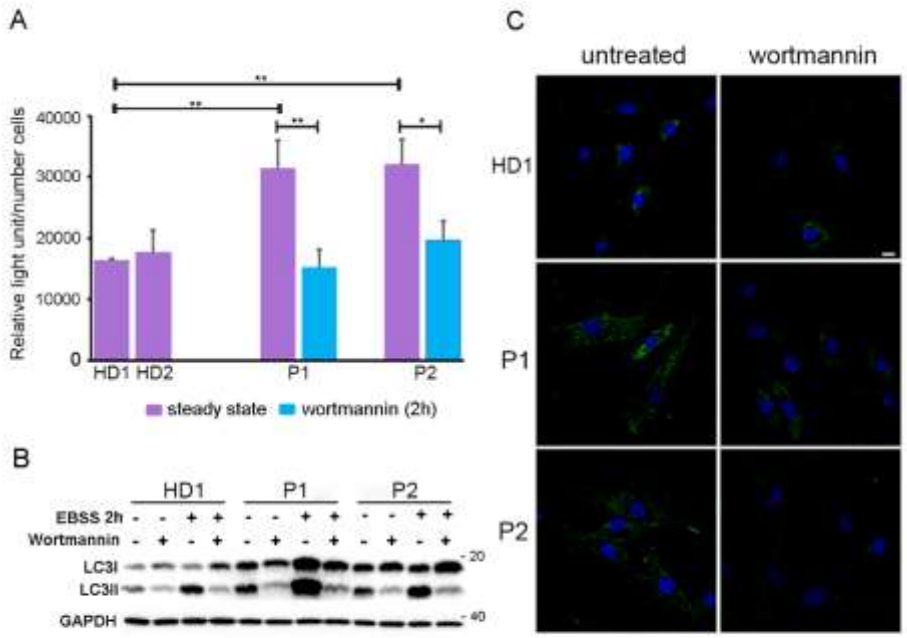

Figure 6. Wortmannin treatment rescues the enhanced glucose uptake and accelerated autophagy in primary fibroblasts from patients with Costello syndrome.

(A) 500 nM wortmannin treatment (2 h) results in a decreased 2DG-glucose intake in patients' cells, comparable to that observed in untreated control cells (HD1). Values are means ± SEM of three independent experiments; *p* values were calculated by one-way ANOVA with Tukey's correction for multiple testing (**p* < 0.05; ***p* < 0.005). **(B)** WB assay performed on patients' fibroblasts treated with 200 nM wortmannin (2 h), in steady state condition or after induction of autophagy with EBSS, shows a decrease of LC3II levels, indicating autophagic flux inhibition. **(C)** Immunofluorescence analysis shows that the decreased glucose uptake associated with wortmannin treatment, promotes lipid droplets consumption. Fixed cells were stained with Bodipy dye (green) and DAPI to visualized nuclei (blue). Scale bar is 48 µm.

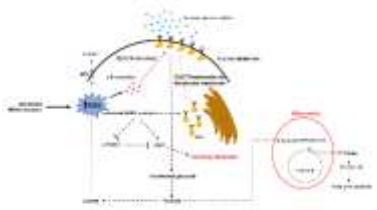

Figure 7. Cartoon summarizing the cascade of events triggered by HRAS-driven elevated ROS levels in primary fibroblasts from patients with Costello syndrome.

According to the proposed model, the increased ROS levels resulting from HRAS functional upregulation results in increased phosphorylation and activation of AMPK and p38, which promote plasma membrane translocation and activation of GLUT4, respectively, resulting in an increased cellular uptake of glucose. In turn, the increased glucose level within cells promotes fatty acid synthesis and their storage as lipid droplets. AMPK activation also promotes autophagy induction in patients' cells, a process that is accelerated in steady state conditions. Solid lines indicate direct effects of increased ROS levels on AMPK and p38 proteins, whereas dashed lines indicate indirect effects on various cellular pathways.